A Two-Way Interactive Nesting Procedure with Variable Terrain Resolution

DA-LIN ZHANG, HAI-RU CHANG, NELSON L. SEAMAN, THOMAS T. WARNER AND J. MICHAEL FRITSCH

Department of Meteorology, The Pennsylvania State University, University Park, PA 16802

(Manuscript received 19 July 1985, in final form 24 January 1986)

ABSTRACT

A two-way interactive, nested-grid system tested with The Pennsylvania State University/NCAR three-dimensional mesoscale model is described. A mesh structure, designed to minimize numerical noise, together with a procedure for obtaining compatible coarse grid mesh (CGM) and fine grid mesh (FGM) terrain conditions, is presented. Also, a method to initialize the nested-grid meshes is proposed. The nested-grid system has been tested with real data and raw terrain under different severe conditions. A 12-h simulation of a propagating jet streak over complex terrain is presented; the results indicate relatively noise-free solutions on both the CGM and FGM domains.

1. Introduction

This paper describes a two-way interactive nesting procedure that has been tested with the Pennsylvania State University/National Center for Atmospheric Research* (PSU/NCAR) mesoscale model originally developed by Anthes and Warner (1978). The primary reason for adding the nesting capability to a numerical model is to improve the horizontal resolution in model forecasts of small-scale atmospheric phenomena or to better resolve large gradients of meteorological variables, without requiring a fine grid mesh (FGM) throughout the entire model domain. The improvement is achieved by resolving smaller-scale features in the FGM, and thereby reducing phase speed errors of medium- and large-scale disturbances and improving the representation of nonlinear transfer processes. However, a compatibility problem exists at the interface where the two grid systems meet. For instance, a disturbance propagating from a coarse grid mesh (CGM) to the FGM may undergo false reflection back to the CGM and scattering into the FGM. On the other hand, a disturbance propagating from the FGM to the CGM may also experience false reflection back onto the FGM or aliasing as it enters the CGM. These interface-generated problems may lead to numerical instabilities that can seriously affect the forecast over the entire domain. This is known as the interface condition problem. An optimal interface procedure that eliminates this problem should have the following properties: 1) all resolvable waves propagate across interfaces smoothly with only minimal changes in amplitude and minimum reflection of energy, and 2) mass, momentum and total energy exchanged between the two grid systems should be conserved. Because of the numerical difficulties involved in the design of a nested grid, procedures which fully satisfy the foregoing two requirements have yet to be described in the literature.

To satisfy the first condition, which is important to allow the nested-grid system to operate effectively, special noise control techniques have to be utilized. Depending on the nature of the modeling problem, noise control techniques used for a two-way system (Phillips and Shukla, 1973) may differ from those used for a one-way approach. For the latter (see Miyakoda and Rosati, 1977), one may employ a radiation condition (Orlanski, 1976) or sponge-type damping (Perkey and Kreitzberg, 1976). Moreover, methods used for a two-way system generally can be applied to the one-way system, but not necessarily vice versa. Methods employed for two-way systems include: (i) selection of a damping time-integration scheme (Phillips, 1978; Kurihara et al., 1979; Ookochi, 1972); (ii) utilization of spatial smoothing operators (Jones, 1977a; Sobel, 1976); (iii) interface adjustment to remove over-specification (Jones, 1977b); (iv) introduction of numerical dissipation into the differencing equation (Kurihara and Bender, 1980; Harrison and Elsberry, 1972) or a combination of these techniques. In a series of three-dimensional experiments, Jones (1977b) found that the spatial smoothers are the most effective method of noise control compared to others he tested. Another approach to efficiently reducing the interface noise is to physically separate the dynamic interface from the mesh interface (e.g., Kurihara et al., 1979; Phillips, 1978). Table 1 presents a summary of features of some existing two-way interactive, nested-grid models. Elsberry (1978) provides further discussions of some nested-grid meshing techniques.

* The National Center for Atmospheric Research is sponsored by the National Science Foundation.

TABLE 1. A summary of some two-way nested grid models.

Model reference	Model type	Interface condition for FGM	Interface condition for CGM	Conservation	Time difference	Space difference	Noise control	Staggered	Terrain	Application
Birchfield (1960)	Nondivergent barotropic	Variable interpolation	Value replacement from FGM at common points	No	Leapfrog	Centered	—	No	No	Real data, 24-h, hurricane movement
Clark and Farley (1984)	Nonhydrostatic P.E.	Variable interpolation	Algorithmic averaging	No	Leapfrog	Arakawa Jacobian	Rayleigh damping	Yes	Yes	Real data, 150-min windstorm
Harrison and Elsberry (1972), Harrison (1973)	Hydrostatic P.E.	Tendency interpolation	Area averaging	No	Leapfrog	Centered	Laplacian diffusion + Euler-backward	No	No	Analytic I.C., 48-h tropical cyclone
Jones (1977a, 1977b)	Hydrostatic P.E.	Tendency interpolation	Nine-point filtering	No	Euler-backward	Centered	Five-point smoother + upstream method	Yes	No	Analytic I.C., 178-h hurricane
Koss (1971)	Shallow water	"Box" method	"Box" method	Mass, momentum	Leapfrog	"Box" method	—	No	No	Analytic I.C. 48-h vortex
Kurihara et al. (1979, 1980)*	Hydrostatic P.E.	"Box" method + variable interpolation*	"Box" method + variable interpolation*	Mass, momentum at dynamic interface**	Two-step iterative	"Box" method	Implicit Newtonian damping	No	No	Analytic I.C. 48-h tropical cyclone
Ookochi (1972)	One-layer shallow water	Variable interpolation	Algorithmic averaging	No	Euler-backward	Arakawa Jacobian type	—	Yes	No	Analytic I.C. 96-h wave evolution
Phillips and Shulka (1973)***	Shallow water	Variable interpolation	Variable interpolation	No	Lax-Wendroff	Centered	—	Yes	No	Analytic I.C., 12-h one-way and two-way comparison
Phillips (1978)***	Hydrostatic P.E.	Variable interpolation	Variable interpolation	No	Lax-Wendroff	Centered	25-point smoother	Yes	Yes	Real data, 48-h hemisphere case study
Sobel (1976)	Hydrostatic P.E.	"Box" method	"Box" method	Mass, momentum	Leapfrog	"Box" method	Time filter + smoother-desmoother	Yes	No	Analytic I.C., 6–12-h jet streak

* Dynamic and mesh interfaces are separated. "Box" method is applied at dynamic interfaces while variable interpolation is performed at mesh interfaces.
** The first moment variables are conserved at dynamic interfaces.
*** Dynamic and mesh interfaces are separated, and variable interpolation occurs within a minimized overlapped annulus.

The assurance of mass and energy conservation across interfaces is a more difficult and challenging problem. It requires that the FGM boundary points be treated as calculation points (i.e., tendencies are computed at the boundary points) and that all fluxes be accumulated with time. Only a few models, such as those developed by Koss (1971), Sobel (1976) and Kurihara et al. (1979) conserve the first-moment properties. By applying the "box" method of Kurihara and Holloway (1967), they developed an appropriate finite difference approximation for the mesh interface. The box method for a staggered grid, as illustrated by Sobel (1976), is extremely complicated because of the irregular shape of "boxes" for momentum points at the mesh interface. Bryan (1966) and Koss (1971) argued the importance of conserving fluxes across interfaces for total energy conservation and control of nonlinear instability. Nevertheless, it may still be necessary to give up the use of a conservative scheme at the interface in order to obtain a smooth solution for the two mesh systems (e.g., Jones, 1977a; Ookochi, 1972). This is particularly true for short-term numerical forecasts in which the use of appropriate model physics and the patterns to be forecast may be more important than exact mass and energy conservation (as long as the mass or energy discrepancy at interfaces is small).

Therefore, the basic strategy adopted was to develop a two-way interactive, nested-grid meshing procedure that is as simple as possible. While the technique described in the following was developed for the PSU/NCAR mesoscale model, the general procedure should be applicable for most primitive equation models. The exact conservation of mass and energy at the interface was sacrificed to circumvent the complicated design for the interface conditions. But this should not be a problem because the finite difference scheme applied on the uniform portion of the grid has been shown to conserve mass and total energy (Anthes and Warner, 1978). The following sections present a simple, but relatively "noise-free," nested-grid meshing technique tested with the PSU/NCAR mesoscale model.

2. Basic model system

The governing equations used in this testing are the same as discussed by Anthes and Warner (1978). The system is hydrostatic in the primitive equations and uses a terrain-following vertical coordinate defined as

$$\sigma = (p - p_t)/p^*, \tag{1}$$

where p is pressure, p_t pressure at the top of the model, $p^* = p_s - p_t$ and p_s the surface pressure. The system is integrated over a staggered grid (lattice B as described by Mesinger and Arakawa (1976)) with horizontal momentum, u, v, defined at dot points and other variables defined at cross points (see Fig. 1). A choice of Lambert conformal, Mercator, or polar sterographic map projections is available.

There are several important additions and improvements of model numerics that have been incorporated into the basic model version described by Anthes and Warner (1978). They are summarized as follows.

- For any variable α, the second-order diffusion $\nabla K_H \nabla \alpha$ was replaced by a more scale-selective, fourth-order operator $\nabla^2(K\nabla^2\alpha)$, where the horizontal eddy viscosity

$$K = K_H \Delta x^2 = A\Delta x^2\left(K_{H0} + \tfrac{1}{2}(k\Delta x)^2|D|\right), \tag{2}$$

where k is von Kármán's constant (0.4) and the deformation of wind D is given by

$$D = \left[\left(\frac{\partial u}{\partial x} - \frac{\partial v}{\partial y}\right)^2 + \left(\frac{\partial v}{\partial x} + \frac{\partial u}{\partial y}\right)^2\right]^{1/2}. \tag{3}$$

The constant K_{H0} depends on mesh size and allows for a background diffusion, and the quantity A is an amplification factor that permits stronger smoothing close to the lateral boundaries. It is defined by

$$A = \begin{cases} 1, & r < r_0 \\ 1 + 3(r - r_0)/\Delta x, & r \geq r_0, \end{cases} \tag{4}$$

where r is the radial distance from the center of the model domain and r_0 is the circular or elliptic radius such that only the four grid points closest to the lateral boundaries sustain an increase of smoothing toward the boundaries. Near lateral boundaries, a second-order diffusion operator is used.

- An implicit vertical diffusion scheme (Richtmyer, 1957) was used under stable conditions, while under conditions of free convection, the Blackadar convective plume model was employed (Zhang and Anthes, 1982). The vertical K-coefficient (K_v) is determined by the Richardson number (Ri) (see Blackadar, 1976; Zhang and Anthes, 1982). This coefficient is given by

$$K_v = K_b + \left|\frac{\partial \mathbf{V}}{\partial z}\right|(kl)^2(R_c - R_i)/R_c \tag{5}$$

where K_b is a background value (1 $m^2 s^{-1}$), l is a constant scale of mixing length (100 m), and R_c is the critical Richardson number

$$R_c = a\Delta z^b \tag{6}$$

where $a = 0.257$, $b = 0.175$ and Δz is the vertical grid increment in meters (see McNider and Pielke, 1981).

- A time-filter (Asselin, 1972) is applied at each time step to all the prognostic variables. It is defined by

$$\hat{\alpha}^\eta = (1 - \nu)\alpha^\eta + \tfrac{1}{2}\nu(\alpha^{\eta+1} + \hat{\alpha}^{\eta-1}) \tag{7}$$

where $\hat{\alpha}$ is the filtered variable and the coefficient ν is 0.1.

• A porous sponge boundary condition (Perkey and Kreitzberg, 1976) was incorporated. It is given by

$$\left.\frac{\partial\alpha}{\partial t}\right|_n = w(n)\left.\frac{\partial\alpha}{\partial t}\right|_{MC} + [1 - w(n)]\left.\frac{\partial\alpha}{\partial t}\right|_{LS} \quad (8)$$

where the subscript MC denotes the model calculated tendency and LS the larger-scale tendency which is specified from observations. The weighting coefficients, $w(n)$, for cross point variables from the CGM boundary inward are 0, 0.4, 0.7, 0.9 and 1, while for dot point variables, they are equal to 0.2, 0.55, 0.8, 0.95. All other interior points for the CGM have $w(n) = 1$.

3. Grid-nesting procedures

a. Mesh structure

Figure 1 shows a schematic of the nested-mesh structure for a two-dimensional (x, y) computational domain. The ratio of grid length and time-step of the CGM to the FGM is 3:1. Because of the staggered-grid structure of the PSU/NCAR model, the next ratio that is geometrically possible is 9:1. However, ratios exceeding 4:1 are generally not recommended for use in two-way interaction since too many FGM points are required to adequately resolve physically meaningful waves on the CGM, and because of the aliasing problem. Vertical levels are identical for the two meshes, but their number and positions can be changed from case to case.

For this nested system, two types of dynamic interfaces are defined: one is the input dynamic interface at which the CGM provides the time-dependent boundary tendencies for the FGM, and another is the feedback dynamic interface at which the predicted FGM values are used to continually update the CGM fields. The input dynamic interface is intentionally separated from the feedback dynamic interface, with the momentum input dynamic interface located coincident with the mesh interface. More details are given in the following subsections. The CGM and FGM domains do not have to be concentric, although the FGM does not move during the forecast. The sizes of the CGM and FGM can be chosen independently.

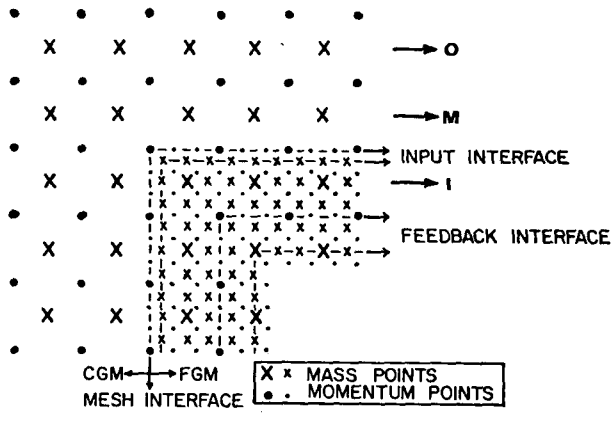

FIG. 1. Portion of nested grid with coarse grid points denoted by large symbols and fine grid points (not coincident with coarse) by small symbols. Letters O, M and I denote the CGM points used to obtain the input interface tendency for the FGM by interpolation (see text).

Integrations proceed from the CGM to the FGM. At the outermost CGM lateral boundaries, the time-dependent tendencies are obtained from the Perkey/Kreitzberg one-way nesting approach. At the input dynamic interface, interpolated CGM tendencies, as will be shown in the next section, are saved for the FGM. Then the FGM fields are advanced three successive time steps until reaching the same time level as the CGM. At this same time level, the computed FGM fields are used to specify CGM field values at coincident points within the feedback dynamic interfaces (see Fig. 1).

b. Interface conditions

The interface conditions are designed to maintain continuity and compatibility of solutions between the two meshes. Following computation of tendencies on the CGM domain, all flux tendencies around the input dynamic interface are saved (one row for momentum along the mesh interface; three rows for mass, labeled O, M and I in Fig. 1). These tendencies are then interpolated along input interfaces for the FGM boundary solution. Because of the nature of the staggered grid, the spatial relationships between CGM and FGM points are different for the mass and momentum variables. For mass points (i.e., p^*, p^*T and p^*q) at the input dynamic interface, tendencies are obtained from a two-step interpolation. First, a Lagrangian interpolation of the CGM tendency between three points perpendicular to the mesh interface (e. g., the points along rows O, M and I in Fig. 1) is made for points at the mass input interface. This is followed by a cubic-spline interpolation along the interface. For momentum points at the FGM boundary, only a cubic-spline interpolation along the interface is necessary. At corners, the FGM tendencies are obtained from a bidirectional interpolation. At first sight, the above process seems to be an overspecification of the FGM boundary conditions. However, the overspecification apparently is slight because the interface solutions for the FGM are almost compatible with solutions over the interior points in terms of physical and dynamic characteristics.

The feedback of FGM fields to CGM fields is obtained at every third time step of the FGM by applying a nine-point operator (Shapiro, 1970) to points interior to the feedback dynamic interface, wherever a CGM point coincides with a FGM point. At this time, the FGM and CGM are at the same time level (i.e., $\eta + 1$). The nine-point operator is given by

$$F_{I,J} = f_{i,j} + \frac{\mu}{2}(1-\mu) \times (f_{i-1,j} + f_{i,j+1} + f_{i+1,j} + f_{i,j-1} - 4f_{i,j}) + \frac{\mu^2}{4}(f_{i-1,j+1} + f_{i+1,j+1} + f_{i+1,j-1} + f_{i-1,j-1} - 4f_{i,j}) \quad (9)$$

where F denotes the value of the coupled variables (e.g., p^*T, $p^*\mathbf{V}$ and p^*q) and p^* at CGM points, f is their values at FGM points and the subscripts I, J define the same CGM position as i, j on the FGM. A value of 0.5 is used for μ.

Therefore, the preceding formulations of interface conditions allow two-way interaction of physical processes to be accomplished: The CGM system provides the FGM with the larger-scale forcing through the input dynamic interface and then the FGM affects the larger scale through the feedback dynamic interface.

It is important here to point out the necessity for separating the input from the feedback dynamic interface. In the first place, the FGM boundary values should not be used for feedback from the FGM to the CGM since the FGM boundary tendencies are specified externally by interpolation from the CGM. By separating the feedback interface, only internally forecast values are used for the feedback calculation. In the second place, if the slight overspecification of the FGM boundary conditions does generate some numerical noise, it will be greatest at points next to the FGM boundary, and thus those points must not be included in the feedback processes.

c. *Treatment of terrain*

Proper treatment of the lower boundary elevation is very important for a nested-grid model since the terrain heights are directly related to mass (p^*) and fluxes (e.g., p^*T, $p^*\mathbf{V}$ and p^*q). In previous applications of a two-way nested grid to meso- or larger-scale dynamics, only Phillips' (1978) model incorporated terrain effects (see Table 1). However, the terrain he used was filtered with a cutoff wavelength of 560 km. In a one-way nested-grid model, Miyakoda and Rosati (1977) found that the model atmosphere was very sensitive to the inclusion of mountainous terrain and that errors and noise tended to be larger in the vicinity of interfaces when complex terrain was used. Numerous tests of the PSU/NCAR nested-grid model not only confirm Miyakoda and Rosati's findings, but show that without special processing of raw terrain data, the noise level increases very rapidly during the first few hours of model integration.

One simple solution to the terrain problem is to use interpolated CGM terrain height for the FGM. However, this approach may not be appropriate in cases where the fine-mesh terrain forcing plays an important role in generating meteorological features of interest. If both coarse-grid and fine-grid terrain data are introduced separately, the resulting FGM terrain field may produce incompatible CGM solutions for mass fields when the feedback processes in the model integration are computed by operator (9). Thus, the problem is how to obtain compatible terrain for the CGM and FGM in the overlap region and also satisfy all computational operations.

A starting point for solving this problem is to require that the final adjusted CGM and FGM terrain values, $H^f_{I,J}$ and $h^f_{i,j}$, respectively, be identical at coincident points in the overlap region (i.e., $H^f_{I,J} = h^f_{i,j}$). An additional constraint is to require that both the CGM and FGM terrain in the entire overlap region simultaneously satisfy the operator (9), i.e., both $H^f_{I,J}$ and $h^f_{i,j}$ at the coincident points are equal to the same nine-point averaged value, $\bar{h}_{i,j}$, of the FGM terrain about i, j. At the surrounding eight points, the adjustment of the terrain height is accomplished as follows.

First, the nine-point operator (9) is applied to the FGM terrain field to determine the averaged values at coincident points,

$$\bar{h}_{i,j} = 0.25h^o_{i,j} + 0.125(h^o_{i+1,j} + h^o_{i-1,j} + h^o_{i,j+1} + h^o_{i,j-1}) + 0.0625(h^o_{i+1,j+1} + h^o_{i+1,j-1} + h^o_{i-1,j+1} + h^o_{i-1,j-1}), \quad (10)$$

where the superscript "o" denotes an original FGM value. In general, the averaged value $\bar{h}_{i,j}$ is not equal to the original FGM value at the coincident points, i.e., $\bar{h}_{i,j} \neq h^o_{i,j}$. The difference is defined by

$$\Delta h = \bar{h}_{i,j} - h^o_{i,j}. \quad (11)$$

Next, a constant, c, is applied to $\bar{h}_{i,j}$ and $h^o_{i,j}$, so that

$$H^f_{I,J} = h^f_{i,j},$$

where

$$H^f_{I,J} = \bar{h}_{i,j} - c\Delta h, \quad (12)$$

$$h^f_{i,j} = h^o_{i,j} + (1-c)\Delta h. \quad (13)$$

The terrain at surrounding FGM points is adjusted by an equal increment, Δz, which is determined as follows

$$\bar{h}_{i,j} - c\Delta h = 0.25[h^o_{i,j} + (1-c)\Delta h] + 0.125(h^o_{i+1,j} + h^o_{i-1,j} + h^o_{i,j+1} + h^o_{i,j-1} - 4\Delta z) + 0.0625(h^o_{i+1,j+1} + h^o_{i+1,j-1} + h^o_{i-1,j+1} + h^o_{i-1,j-1} - 4\Delta z). \quad (14)$$

Using relation (10), and rearranging, one gets

$$\Delta z = \left(c + \frac{1}{3}\right)\Delta h. \quad (15)$$

Several choices can be derived from the above relation (see Zhang, 1985). We choose $c = 0$, and $\Delta z = \Delta h/3$. That is, the FGM and CGM terrain heights at the coincident points are adjusted to the nine-point smoothed

value, $\bar{h}_{i,j}$, while the surrounding eight FGM points are altered by amount $-\Delta h/3$. Comparisons of the FGM terrain after the above manipulation with that before the processing show small differences in magnitude. In fact, the mean and the standard deviation of height changes for a typical Appalachian case are 0 and 3.9 m, respectively. These modest changes are not important compared to the uncertainties associated with the original terrain data and objective analysis processes.

d. Noise control

Most finite-differenced primitive equation models require some means of controlling spurious growth of short-wavelength energy. In the unnested PSU/NCAR model, implicit vertical diffusion is very effective in damping large vertical gradients or discontinuities, and high frequency noise is controlled by the use of the Asselin time filter. Horizontally oriented short-wave oscillations are removed by a diffusion operator [see Eqs. (2)–(4)].

However, nested-grid models usually exhibit additional numerical noise near interfaces due to the nonuniform nature of the meshed grid. In this model, the fourth-order horizontal diffusion [Eqs. (2)–(4)] with the diffusion coefficient increasing toward lateral boundaries is used to suppress quasi-stationary short-wave noise on both grids. Also, the technique described in section 3c minimizes noise produced by terrain-character incompatibilities between the CGM and FGM. Nevertheless, in early tests of a prototype nesting technique using the 10–11 May 1973 jet streak case (Uccellini and Johnson, 1979; Brill et al., 1985), in which an upper-level jet was allowed to propagate across the nest interface, the solution was noisy near the interface. This noise was significantly reduced by physical separation of the input from the feedback dynamic interfaces. However, owing to the slight overspecification of the surface pressure tendency at the input dynamic interface when used to compute the vertical motion in σ coordinates, $\dot{\sigma}$, there tends to be positive feedback between the $\dot{\sigma}$ and momentum convergence in the FGM domain. The consequent noise in the three-dimensional winds increases with height and eventually can lead to numerical instability.

In order to control the effects of the incompatibility of the CGM and FGM solutions at the interface, a Newtonian-type damping scheme, similar to the one used by Kurihara and Bender (1980), is applied to the FGM momentum points next to the nest interface. That is,

$$\frac{\partial p^*\mathbf{V}}{\partial t} = \cdots - (p^*\mathbf{V} - \overline{p^*\mathbf{V}})^{\tau+1}/\tau_d(\sigma) \qquad (16)$$

where $\tau_d(\sigma)$ is the relaxation time as a function of height. The relaxation time has a magnitude of $20\Delta t$ at the topmost layer and $100\Delta t$ at the lowest layer. Using the latest time level, we obtained the reference value, $\overline{p^*\mathbf{V}}$, from a two-point average, using values at the points on either side of the point being adjusted and along the line normal to the interface (e.g., the FGM input dynamic interface point and the third point from the interface).

Very little noise is generated over the domain of the CGM and is easily controlled by the conventional techniques. This is partly because of the relatively weak convergence-divergence which develops on the CGM, and partly because the inertial–gravity waves associated with any noise in the CGM tend to dissipate before they reflect at the CGM boundary. Also, the nine-point operator used for feedback from the FGM [Eq. (9)] helps to prevent noise that could occur when FGM short waves are represented on the CGM.

4. Initialization

It is highly desirable that the initial conditions of the FGM and the CGM be determined in such a way that the fields in the overlap region are compatible when integration begins. When sufficient observations are available, it is also desirable that the initialization procedure retain as much detail as possible over the entire FGM domain (Elsberry and Ley, 1976). The procedure for obtaining the grid point values starts with the CGM. A first guess is obtained from the operational analysis fields from the National Meteorological Center (NMC). Specifically, the NMC global or northern hemispheric octagonal grid data are horizontally interpolated to the grid points of the CGM domain using a 16-point Bessel formula. These data include sea-level pressure and surface temperature plus mandatory level horizontal wind, temperature and relative humidity. These fields are then vertically interpolated to an arbitrary selection of "model" significant levels. All these "first guess" fields at both mandatory and significant levels are then enhanced with the standard rawinsonde station soundings and bogus soundings using a successive-correction type of objective analysis technique (Benjamin and Seaman, 1985).

The next step in obtaining the CGM grid point values is to interpolate all three-dimensional fields from pressure surfaces to model sigma surfaces. If desired, the mass field can be balanced to the rotational component of the wind field, or the vertically integrated divergence in a column can be removed from the wind field (Washington and Baumhefner, 1975) in order to minimize noise early in the forecast. At this stage, the initial conditions for the CGM are complete except for the region where the CGM overlaps with the FGM. For that region, all CGM initial conditions need to be determined after the FGM initialization is complete.

For the FGM, a first guess at all pressure levels is obtained directly from horizontal interpolations of the enhanced CGM fields using a two-dimensional bicubic

spline. When there are few or no additional data for fine-resolution analysis on the FGM, this first guess is acceptable as the final FGM initial analysis. For cases in which finer resolution data are available, this first guess is then enhanced with the observations and bogus soundings occurring in the FGM domain. In order to attain better quality interface conditions, the FGM domain is temporarily extended for the objective analysis phase (i.e., three grid lengths outward from the perimeter of the original FGM). The same objective analysis procedures as for the CGM are then followed. For cases in which a new FGM mesoscale analysis is performed, the final step is to obtain the CGM fields in the overlap region. They are determined from the FGM counterparts using the nine-point operator, in the same way as the feedback computation described in Section 3b. Meanwhile, the extended parts of the FGM are removed before numerical integration proceeds.

5. Example of nesting tests

While detailed case applications of this nested-grid model will appear in subsequent publications, it is necessary to demonstrate its general response, especially in the region of the nest interface. Figures 2–5 show some preliminary results from a 12-h nested-grid simulation of the 10–11 May 1973 jet streak. The coarse grid consisted of 37 × 37 points spaced at 120 km and the fine grid had 37 × 37 points at intervals of 40 km. The model was run with 10 equally spaced layers with the top at 100 mb. This experiment was conducted with a one-layer bulk aerodynamic boundary layer and

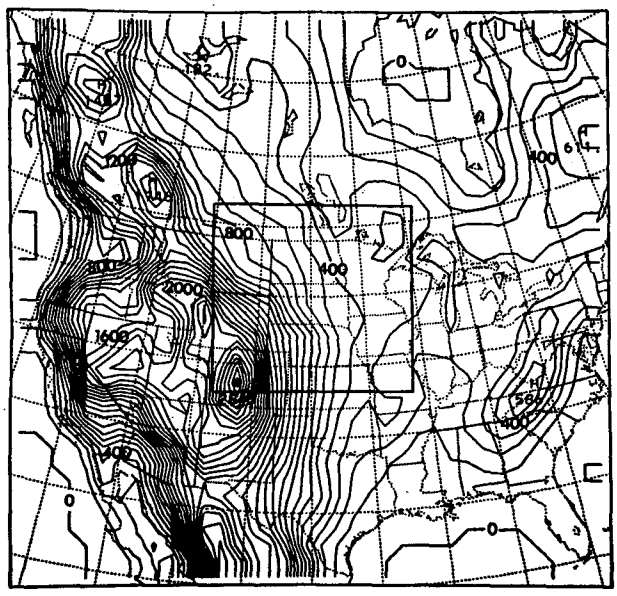

FIG. 2. Terrain field of the CGM used for the jet streak case (contour interval 100 m). The interior thick solid lines denote the nest interface.

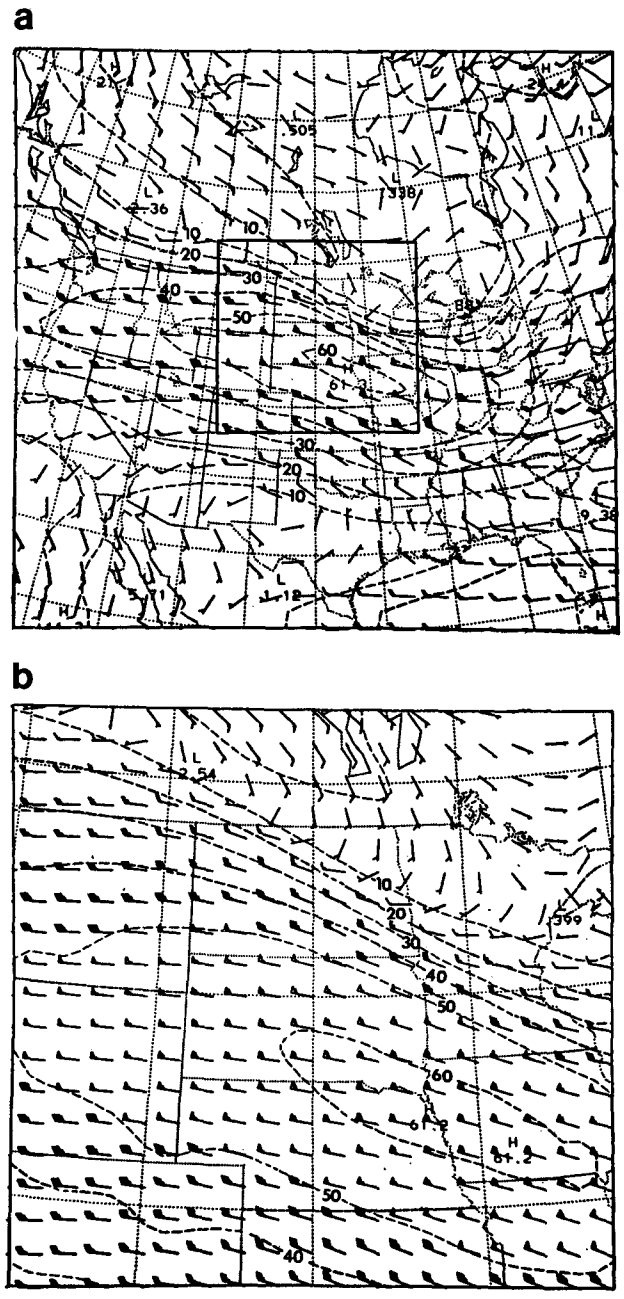

FIG. 3. Twelve hour forecast conditions of 325 mb horizontal wind (V, m s^{-1}) at 0000 GMT 11 May 1973 for (a) the CGM and (b) the FGM.

with an R. A. Anthes/H. L. Kuo type cumulus parameterization scheme (see Anthes and Keyser, 1979). The reader is referred to Uccellini and Johnson, 1979; Brill et al., 1985; and Seaman et al., 1985, for a more detailed description of this case. In this experiment the nest interface was purposely chosen to lie near the highest terrain of the Rocky Mountains in Colorado (see Fig. 2). An upper-level jet streak crossed the inflow interface

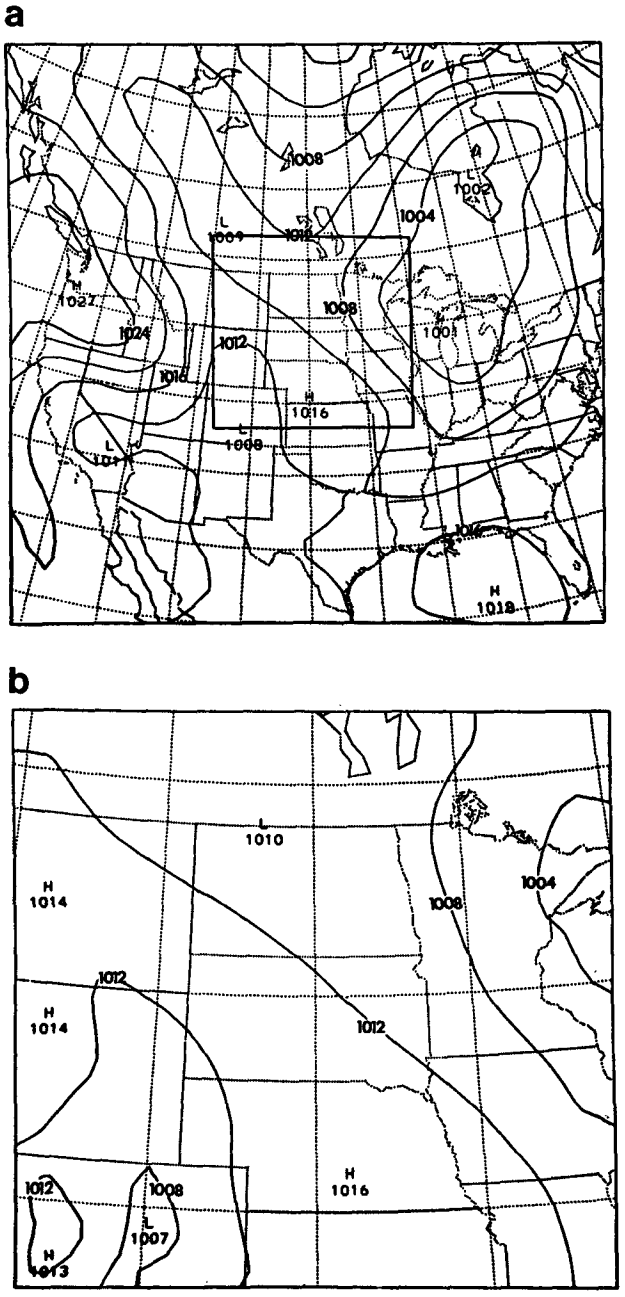

FIG. 4. Twelve-hour forecast of (a) the CGM and (b) FGM sea-level pressure (P_{sea}, mb) at 0000 GMT 11 May 1973.

and then approached the outflow interface. Thus, both the meteorological and orographic forcing provide severe tests for the nested-grid model, particularly for the nest interface.

Comparisons of Figs. 3–5 with analyses and coarse-resolution forecasts (see Uccellini and Johnson, 1979; Brill et al., 1985; and Seaman et al., 1985) show that the propagation of the jet streak and its associated features were simulated well by the nested-grid model. There are no spurious distortions evident in the vicinity of the interface. Because of the complex terrain, there were local perturbations in most meteorological variables. These perturbations are considered to be more or less physically consistent with orographic disturbances of stable flows. In particular, a mesohigh–mesolow couplet developed at the southwestern corner of the FGM (see Fig. 4b). This is physically associated with the upwind-blocking and lee-troughing commonly observed in the vicinity of the Rocky Mountains. Associated mountain-wave perturbations can also be seen in the horizontal and vertical winds (see Figs. 3b and 5). Similar, but weaker, orographically induced perturbations are found for an unnested experiment with only the 120-km coarse mesh (not shown). It is important to point out that there was no significant noise at the penultimate row of points which is frequently the site of spurious wave disturbances in nested-grid models with ill-posed interface conditions. Further evidence of the numerical and physical consistency of the nested-grid model can be found by examination of the 500 mb vertical motion field ω (see Fig. 5). This variable is normally sensitive to both standing and propagating wave energy. Notice that the only distinct features are clearly associated with the mountain wave in Colorado and the jet streak over the plains, even though these are not very strong circulations. No important noise is apparent.

In addition to the foregoing jet-streak test, other severe tests have been performed to check the feasibility of the nesting techniques. These include a study in which deep convection and associated strong convergence developed near the interface (see Seaman et al.,

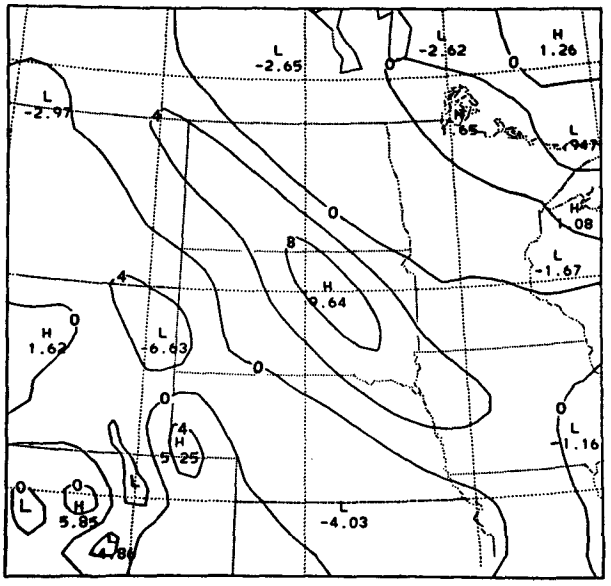

FIG. 5. Vertical motion (ω, μb s^{-1}) at 500 mb for 12 h forecast of the FGM at 0000 GMT 11 May 1973.

1985). In another study, in which Δx in the FGM was 25 km, meso-β scale highs, lows and intense convection approached the interface and a midtropospheric meso-α scale short wave propagated across the interface (see Zhang, 1985; Zhang and Fritsch, 1986). In all these studies, all meteorological fields remained smooth on both the CGM and FGM and wave distortions at the interface remained small. Detailed illustrations of these results will be published in forthcoming journal articles.

6. Summary

A two-way interactive, nested-grid system tested with the PSU/NCAR mesoscale model has been described. The mesh structure is designed with a feedback dynamic interface that is separated from an input dynamic interface. The momentum input interface is located coincident with the mesh interface. A procedure for obtaining compatible CGM and FGM terrain conditions has been developed. This procedure permits the successful incorporation of realistic complex terrain, and allows mass to be conserved between the two meshes. Because the vertical motion in σ coordinates, $\dot{\sigma}$, is computed at the FGM boundary but the surface pressure tendency needed to compute $\dot{\sigma}$ is specified from the CGM computation, a weak Newtonian-type noise-suppression scheme with coefficient increasing with height is applied to the FGM momentum computation at points next to the mesh interface. Otherwise, the numerical noise control mechanisms used for the unnested model are sufficient. The initialization procedure begins by specifying the CGM conditions using the NMC analysis as a first guess and then enhancing this analysis with the standard rawinsonde observations and bogus data. The FGM is initialized using the CGM interpolated values as a first guess and these values are enhanced using observed and bogus soundings.

This nesting procedure has been tested with real data under different severe conditions. In a typical case presented here, a 12-h simulation of a propagating jet streak over complex terrain showed relatively noise-free solutions for both the CGM and FGM. Preliminary experiments indicate that the compatible CGM and FGM terrain conditions, the separation of the feedback from input dynamic interface and the use of a short-wave filter at the nest interface made significant contributions to the relatively noise-free solutions. More experiments to severely test additional aspects of the nesting techniques are under way and will be described in a future paper.

Acknowledgments. This work was supported by NSF Grants ATM-8218208 and ATM-811323 and by the Electrical Power Research Institute via Contract RP1616-28. Computer support was provided by the National Center for Atmospheric Research, which is sponsored by the National Science Foundation. The authors gratefully acknowledge Mrs. Delores Corman for skillfully preparing the manuscript.

REFERENCES

Anthes, R. A., and T. T. Warner, 1978: Development of hydrodynamic models suitable for air pollution and other mesometeorological studies. *Mon. Wea. Rev.*, **106,** 1045–1078.

——, and D. Keyser, 1979: Tests of fine-mesh model over Europe and the United States. *Mon. Wea. Rev.*, **107,** 963–984.

Asselin, R., 1972: Frequency filter for time integration. *Mon. Wea. Rev.*, **100,** 487–490.

Benjamin, S. G., and N. L. Seaman, 1985: A simple scheme for objective analysis in curved flow. *Mon. Wea. Rev.*, **113,** 1184–1198.

Birchfield, G. E., 1960: Numerical prediction of hurricane movement with the use of fine grid. *J. Meteor.*, **17,** 404–414.

Blackadar, A. K., 1976: Modeling the nocturnal boundary layer. *Preprints Third Symp. on Atmospheric Turbulence, Diffusion and Air Quality,* Raleigh, Amer. Meteor. Soc., 46–49.

Brill, K. F., L. W. Uccellini, R. P. Burkhart, T. T. Warner and R. A. Anthes, 1985: Numerical simulations of a transverse indirect circulation and low-level jet in the exit region of an upper-level jet. *J. Atmos. Sci.*, **42,** 1306–1320.

Bryan, K., 1966: Scheme for numerical integrations of equations of motion on an irregular grid free of non-linear instability. *Mon. Wea. Rev.*, **94,** 39–40.

Clark, T. L., and R. D. Farley, 1984: Severe downslope windstorm calculations in two and three spatial dimensions using anelastic interactive grid nesting: A possible mechanism for gustiness. *J. Atmos. Sci.*, **41,** 329–350.

Elsberry, R. L., 1978: Prediction of atmospheric flows on nested grids, *Computational Techniques for Interface Problems,* AMD-Vol. 30, 67–86. [Available from Amer. Soc. Mech. Eng., 345 E. 47th Street, New York, NY 10017.]

——, and G. W. Ley, 1976: On the strategy of initializing nested grid meshes in numerical weather prediction. *Mon. Wea. Rev.*, **104,** 797–799.

Harrison, E. J., 1973: Three-dimensional numerical simulations of tropical systems utilizing nested finite grids. *J. Atmos. Sci.*, **30,** 1528–1543.

——, and R. L. Elsberry, 1972: A method for incorporating nested finite grids in the solutions of systems of geophysical equations. *J. Atmos. Sci.*, **29,** 1235–1245.

Jones, R. W., 1977a: A nested grid for a three-dimensional model of a tropical cyclone. *J. Atmos. Sci.*, **34,** 1528–1553.

——, 1977b: Noise control for a nested grid tropical cyclone model. *Contrib. Atmos. Phys.*, **50,** 393–402.

Koss, W. J., 1971: Numerical integration experiments with variable-resolution two-dimensional Cartesian grids using the box method. *Mon. Wea. Rev.*, **99,** 725–738.

Kurihara, Y., and J. L. Holloway, 1967: Numerical integration of a nine-level global primitive equations model formulated by the box method. *Mon. Wea. Rev.*, **95,** 509–530.

——, and M. A. Bender, 1980: Use of a movable nested-mesh model for tracking a small vortex. *Mon. Wea. Rev.*, **108,** 1792–1809.

——, G. J. Tripoli and M. A. Bender, 1979: Design of a movable nested-mesh primitive equation model. *Mon. Wea. Rev.*, **107,** 239–249.

McNider, R. T., and R. A. Pielke, 1981: Diurnal boundary-layer development over sloping terrain. *J. Atmos. Sci.*, **38,** 2198–2212.

Mesinger, F., and A. Arakawa, 1976: Numerical methods used in atmospheric models. GARP Publication Series No. 17, 64 pp. [WMO/ICSU, Case Postale No. 5, Ch-1211, Geneva 20, Switzerland.]

Miyakoda, K., and A. Rosati, 1977: One-way nested models: The

interface conditions and the numerical accuracy. *Mon. Wea. Rev.*, **105**, 1092–1107.

Ookochi, Y., 1972: A computational scheme for the nesting fine mesh in the primitive equation model. *J. Meteor. Soc. Japan*, **50**, 37–48.

Orlanski, I., 1976: A simple boundary condition of unbounded hyperbolic flows. *J. Comput. Phys.*, **21**, 251–269.

Perkey, D. J., and C. W. Kreitzberg, 1976: A time-dependent lateral boundary scheme for limited-area primitive equation models. *Mon. Wea. Rev.*, **104**, 744–755.

Phillips, N. A., 1978: The nested grid model. NOAA Tech. Rep., NMC, 80 pp. [Available from ESIC(D822), NOAA, 6009 Executive Blvd., Rockville, MD 20852.]

——, and J. Shukla, 1973: On the strategy of combining coarse and fine grid meshes in numerical weather prediction. *J. Appl. Meteor.*, **12**, 763–770.

Richtmyer, R. D., 1957: Difference methods for initial-value problems, *Interscience*, 283 pp.

Seaman, N. L., H.-R. Chang, D. R. Stauffer and T. T. Warner, 1985: Simulations of mesoscale meteorology with a nested-grid numerical prediction model. *Preprints Seventh Conf. on Numerical Weather Prediction*, Amer. Meteor. Soc., 251–258.

Shapiro, R., 1970: Smoothing, filtering and boundary effects. *Rev. of Geophys. Space Phy.*, **8**, 359–387.

Sobel, J. P., 1976: Nested grids in numerical weather prediction and an application to a mesoscale jet streak. Ph.D. thesis, The Pennsylvania State University, 135 pp.

Uccellini, L. W., and D. R. Johnson, 1979: The coupling of upper and lower tropospheric jet streaks and implications for the development of severe convective storms. *Mon. Wea. Rev.*, **107**, 682–703.

Washington, W. M., and D. P. Baumhefner, 1975: A method of removing Lamb waves from initial data for primitive equation models. *J. Appl. Meteor.*, **14**, 114–119.

Zhang, D.-L., 1985: Nested-grid simulation of the meso-β scale structure and evolution of the Johnstown flood of July 1977. Ph.D. thesis, The Pennsylvania State University, 270 pp.

——, and R. A. Anthes, 1982: A high-resolution model of the planetary boundary layer—sensitivity tests and comparisons with SESAME-79 data. *J. Appl. Meteor.*, **21**, 1594–1609.

——, and J. M. Fritsch, 1986: Numerical simulation of the meso-β scale structure and evolution of the 1977 Johnstown flood. Part I: Model description and verification. *J. Atmos. Sci.* (in press).